A Combinational Effect of "Bulk" and "Surface" Shape-Memory Transitions on the Regulation of Cell Alignment

*Koichiro Uto, Takao Aoyagi, Cole A. DeForest, Allan S. Hoffman, and Mitsuhiro Ebara**

A novel shape-memory cell culture platform has been designed that is capable of simultaneously tuning surface topography and dimensionality to manipulate cell alignment. By crosslinking poly(ε-caprolactone) (PCL) macromonomers of precisely designed nanoarchitectures, a shape-memory PCL with switching temperature near body temperature is successfully prepared. The temporary strain-fixed PCLs are prepared by processing through heating, stretching, and cooling about the switching temperature. Temporary nanowrinkles are also formed spontaneously during the strain-fixing process with magnitudes that are dependent on the applied strain. The surface features completely transform from wrinkled to smooth upon shape-memory activation over a narrow temperature range. Shape-memory activation also triggers dimensional deformation in an initial fixed strain-dependent manner. A dynamic cell-orienting study demonstrates that surface topographical changes play a dominant role in cell alignment for samples with lower fixed strain, while dimensional changes play a dominant role in cell alignment for samples with higher fixed strain. The proposed shape-memory cell culture platform will become a powerful tool to investigate the effects of spatiotemporally presented mechanostructural stimuli on cell fate.

1. Introduction

There has been widespread interest from basic biology to medical science toward understanding how cell fate is regulated in the human body. In general, determination of cellular processes such as growth, proliferation, and differentiation is governed by a complex set of extrinsic cues in collaboration with intrinsic gene regulatory machinery. Among them, an increasing number of studies have shown that the mechanostructural stimuli including elasticity, topography, and mechanical force alter cell differentiation and tissue growth. For example, mechanical forces between a cell and the substrate can affect many cellular functions, including cell proliferation and apoptosis.[1,2] It has also been reported that differentiation behaviors of mesenchymal stem cells (MSCs) are highly sensitive to substrate stiffness.[3,4] Cell functions are also affected by topographical features such as grooves, pores, and ridges in micro- or nanoscale, attributed to similarities with fibral structurals comprising the extracellular matrix (ECM). Kim and co-workers have constructed a nanotopographically controlled model of myocardium mimicking the ventricular organization and revealed that cell geometry, action potential conduction velocity, and the expression of a cell–cell coupling protein were extremely sensitive to differences in the substratum nanoscale features of the surrounding ECM.[5] Osteogenic differentiation of human MSCs was also enhanced when they were cultured on nanostructured surfaces.[6] It is also known that the alignment of MSCs or progenitor cells is an intrinsic cue for differentiation.[7–10] These studies suggest that gene expression programs and cellular signaling for directing cell fate are guided by extrinsic mechanostructural cues that are propagated through the cytoskeleton.

Recent progress in developing bioengineering and nanofabrication techniques has enabled materials that present key regulatory signals to control cell functions; there has recently been significant effort to transition from traditional "static" biomaterials toward new "dynamic" biomaterials that provide specialized cell behavioral cues in temporally defined manners.[11–15] Indeed, the concentration, distribution, and dynamic interaction of molecules that occur within our bodies are responsible for tissue morphogenesis and maintained homeostasis. Time has also been shown to be an important factor which determines stem cell fate.[16,17] Therefore, "dynamic" biomaterials not only provide structural support but also play important regulatory roles in controlling extracellular microenvironmental cues to guide the cell behavior and formation of functional tissues. In this context, "smart" or "stimuli-responsive" materials have emerged as powerful tools for basic cell studies and have shown promise in a variety of biomedical applications. Recent examples of smart materials

Dr. K. Uto, Prof. T. Aoyagi, Dr. M. Ebara
International Research Center for Materials Nanoarchitectonics (WPI-MANA)
National Institute for Materials Science (NIMS)
1-1 Namiki, Tsukuba 305-0044, Japan
E-mail: ebara.mitsuhiro@nims.go.jp
Prof. C. A. DeForest
Department of Chemical Engineering
University of Washington
4000 15th Ave NE, Seattle, WA 98195, USA
Prof. Emer. A. S. Hoffman
Department of Bioengineering
University of Washington
3720 15th Ave NE, Seattle, WA 98195, USA

DOI: 10.1002/adhm.201601439

include temperature-responsive polymer surfaces, where the surface energy can be controlled with temperature.[18–22] Concerning dynamically switchable surfaces with mechanostructural properties, Takayama and co-workers have developed a reconfigurable microtopography system for cell alignment using reversible wavy microfeatures on poly(dimethylsiloxane) (PDMS).[23] Tanaka and co-workers have recently demonstrated a thin, stimulus-responsive hydrogel that permitted reversible adjustment of the mechanical environment and the dynamic morphological transition of cell caused by cell–substrate contacts dependent on substrate elasticity.[24] Recently, an interesting phenomenon denoted mechanical "memory" has been observed, where hydrogel substrates with dynamically tunable mechanical properties have been used to demonstrate that stem cells remember physical signals from their past culture.[25,26]

In this work, we propose to utilize a shape-memory culture platform where the substrate induces mechanical deformation similar to that which cells experience within the dynamic in vivo environment. Shape-memory polymers (SMPs) are a class of "smart" materials that have the capability to change from one or more temporary states to a permanent shape upon application of an external stimulus.[27–29] Most previous works for shape-memory cell culture platforms have centered on "surface" shape memory behavior.[30–32] We have reported shape-memory surfaces fabricated from temperature-responsive poly(ε-caprolactone) (PCL) films with on-demand, tunable nanopatterns, which were developed to observe time-dependent changes in cell alignment.[32–35] On the other hand, there are only a few reports which addressed the "bulk" shape-memory effect on cell functions due to the fact that a large dimensional change of cell culture substrate during shape-memory transition induces cell detachment or apoptosis.[36] In this study, we develop a shape-memory cell culture film that undergoes preprogrammed changes in combined "surface" topography and "bulk" dimension in a near-physiological fashion (**Figure 1**a). Since shape-memory-induced alterations in material topography can originate from changes within or on the surface of a material, we respectively denoted these as "bulk" and "surface" shape-memory effects to aid in our analysis. Furthermore, we quantitatively analyzed cell alignment on the films with various deformation ratios before and after the shape-memory activation, the surface of which was programmed to transit from an elongated temporal shape with or without nanowrinkled surface to a flat original shape (Figure 1b).

2. Results

2.1. "Bulk" Shape-Memory Behavior—Dimensional Changes

To develop biocompatible SMPs that actuate sharply in a narrow range near body temperature, we have recently reported a simple and versatile protocol to modulate the T_m of crosslinked PCLs by varying the mixing ratio of PCL macromonomers with two- (2*b*) and four-branched (4*b*) arms (Figure S1 in the Supporting Information).[32,37] Chemical crosslinking prevents the polymers from de-entangling and allows improved shape recovery. In this study, a PCL film composed of equimolar amounts of 2*b* and 4*b* macromonomers was selected due to its compatability with live cell culture (T_m around 33 °C). The shape-memory transition occurred over a 5 °C temperature range and is associated with a large elastic and compression modulus change from 26.4 ± 2.7 to 0.9 ± 0.1 and 11.7 ± 0.1 to 5.8 ± 0.1 MPa, respectively, while surface wettability was independent of incubation temperature (≈98° estimated by contact angle measurement). The characteristics of the crosslinked PCL films are summarized in Table S1 and Figure S3 (Supporting Information).

Figure 1b shows a schematic depiction of the programming and recovery of the shape-memory PCL films by processing through heating, stretching, and cooling. In the first step, the sample was deformed at a temperature above T_m, resulting in a linear increase of strain in a range from 0% to 100% of the original shape (deformation process). In the second step, the sample was cooled below the crystallization temperature

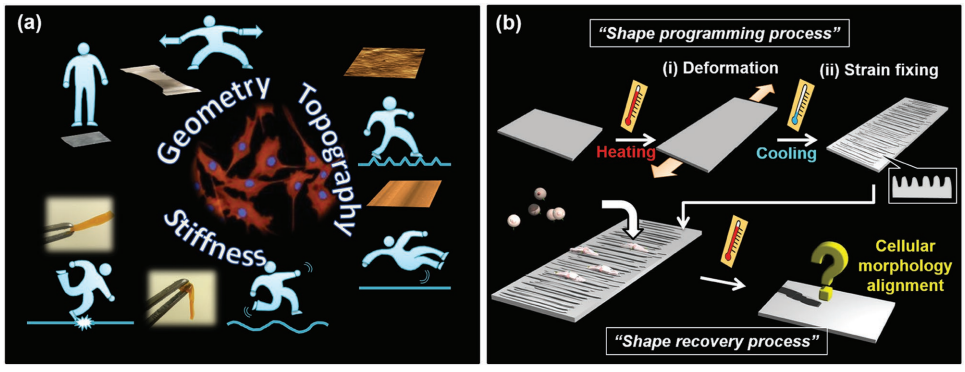

Figure 1. a) Mechanostructural stimuli such as stiffness, topography, and geometry alter functions of a number of tissues and cells. Shape-memory PCL enables to induce programmed cell alignment by dynamically transforming the surface topography, dimension, and network mechanics in response to temperature change. b) Schematic representation of shape fixing and recovery processes of the shape-memory PCL film. To program temporary shapes, the films were elongated in thermo-chamber. Predetermined strain (0%–100%) was applied to the samples at 40 °C (above the melting temperature (T_m)). The applied strain was then fixed at 4 °C (below crystallization temperature (T_c)) for 30 min of cooling. In the films with lower fixed strain, the nanowrinkle emerged on the surface of crosslinked PCL as shown in illustrations. Samples had a temporary strain fixed shape that could be triggered to transition to the original shape by heating.

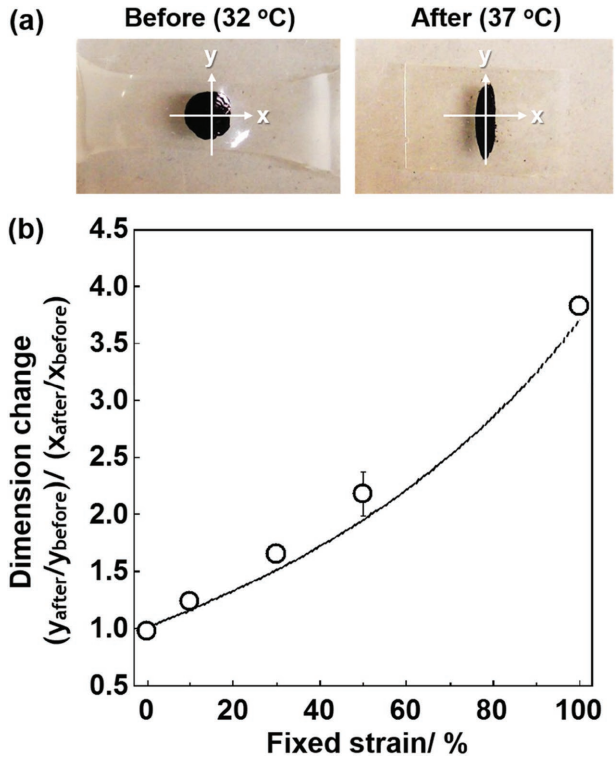

Figure 2. Dimensional change of strain fixed PCL film by shape-memory activation. a) Photographs of crosslinked PCL with 100% fixed strain before and after shape-memory activation by heating at 37 °C for 1 h. After strain fixing of crosslinked PCL, the film was marked with a black dot (diameter of 5 mm) by pen to quantitatively estimate the dimension change during shape-memory activation. b) Dimension change of crosslinked PCL with various fixed strain by shape-memory activation. Dimension changes were calculated from the length ratio of X axis (elongation direction) and Y axis (perpendicular direction against elongation) before and after shape-memory activation (error bars are standard deviation from $n = 3$ experiments). Solid line shows the theoretical relationship between the dimension change and fixed strain calculated using an assumed Poisson's ratio (ν) of crosslinked PCL of 0.46.

(T_c) of 4 °C under constant stress to fix the extended strain. Quantitative shape-memory properties including shape fixity (R_f) and shape recovery (R_r) are investigated by cyclic thermomechanical analysis. The crosslinked PCL film exhibits excellent shape fixity and recovery, where R_f (first cycle) and R_f (fifth cycle) were ≈98% and 100%, and R_r (1) and R_r (5) were ≈90% and 98%, respectively.

Dimensional deformation of PCL films before and after shape-memory activation was studied (**Figure 2**a). Figure 2b plots the difference in dimensional changes of PCL films against the prefixed strain. The dimensional changes were determined from their lateral and longitudinal lengths and increased proportionally with increased fixed strain. This result also indicates the excellent shape-fixing ability of the crosslinked PCL. These experimental values were also compared with the theoretical values calculated using an assumed Poisson's ratio of crosslinked PCL ($\nu = -d\varepsilon_y/d\varepsilon_x = 0.46$, where $d\varepsilon_x$ and $d\varepsilon_y$ are the change of x-axis (longitudinal) and y-axis (transverse) strain, respectively).[38,39]

2.2. "Surface" Shape-Memory Behavior—Topographical Changes

Figure 3a,b shows the atomic force microscope (AFM) images of the surface morphologies on prestretched PCL films of various strain fixity measured over an area of 50 × 50 μm^2. Below T_m, irregular rough surface was observed for a nonstretched film (0%), while the surface became smooth above T_m as the region of high crystallinity transitioned to amorphous phase. When an original PCL film was elongated to 10% strain, on the other hand, the formation of nanowrinkle structures was observed. These wrinkles were nanometer sized, buckled perpendicular to the elongation direction, and relatively aligned (Figure S4 in the Supporting Information). Of particular interest is that the surface roughness R_a decreased with increasing strain below T_m (Figure 3c). The measured R_a values were found to be 102.4 ± 21.2, 90.8 ± 13.6, 79.1 ± 9.9, and 21.3 ± 9.8 nm for 10%, 30%, 50%, and 100% of fixed strain, respectively. In addition, the wrinkles were found to be disordered when the film was elongated to 50% of strain and wrinkle structures were difficult to observe for strain of 100% (Figure S4, Supporting Information). These nanowrinkled structures disappeared to yield flat surfaces when materials temperature was raised above T_m, regardless of strain fixity values (Figure 3b,c).

To examine this nanowrinkled formation mechanism, we evaluated the contraction stress during the strain fixing (cooling) process as shown in **Figure 4**a,b. This stress was originally attributed to crystallization of PCL chains. The larger contraction stress of the PCL during the strain fixing process was observed for samples with lower fixity strain. This result is consistent with the observed trends in surface roughness versus strain fixity. The contraction stress was negligible for 100% strain because the magnitude of the compressive stress was smaller than the stretched tension stress and the substrate was unable to shrink to form any surface wrinkle structure (Figure 4c).

2.3. Response of Cells to Shape-Memory Activation

To investigate the role of "dynamic" changes in surface topography and dimension on cell functions, specifically cell alignment, cells were cultured on shape-memory PCL films and both "bulk" and "surface" shape-memory activations were carried out. First, NIH3T3 fibroblasts were seeded on fibronectin-coated PCL films and cultured at 32 °C for 24 h (**Figure 5**a). Before cell cultivation, PCL films were elongated and fixed at various strains. Since the shape-memory transition occurs above 33 °C, the temporary shape is stable over culture temperatures at or below 32 °C. Cells adhered and spread well on the surfaces regardless of strain-fixity values. The cells seeded on the substrates with 10% and 30% of initial strains elongated parallel with the nanowrinkles. In contrast, cells on the substrates with 50% and 100% of initial strains exhibit random orientation. These results correlated well with the surface topographic features of the underlying substrates observed by AFM (Figure 3).

Next, the cultured cells were transferred to a 37 °C incubator after 24 h of incubation at 32 °C and shape-memory activation was allowed. Figure 5b exhibits cell morphologies after the shape-memory activation. We observed that all cells were

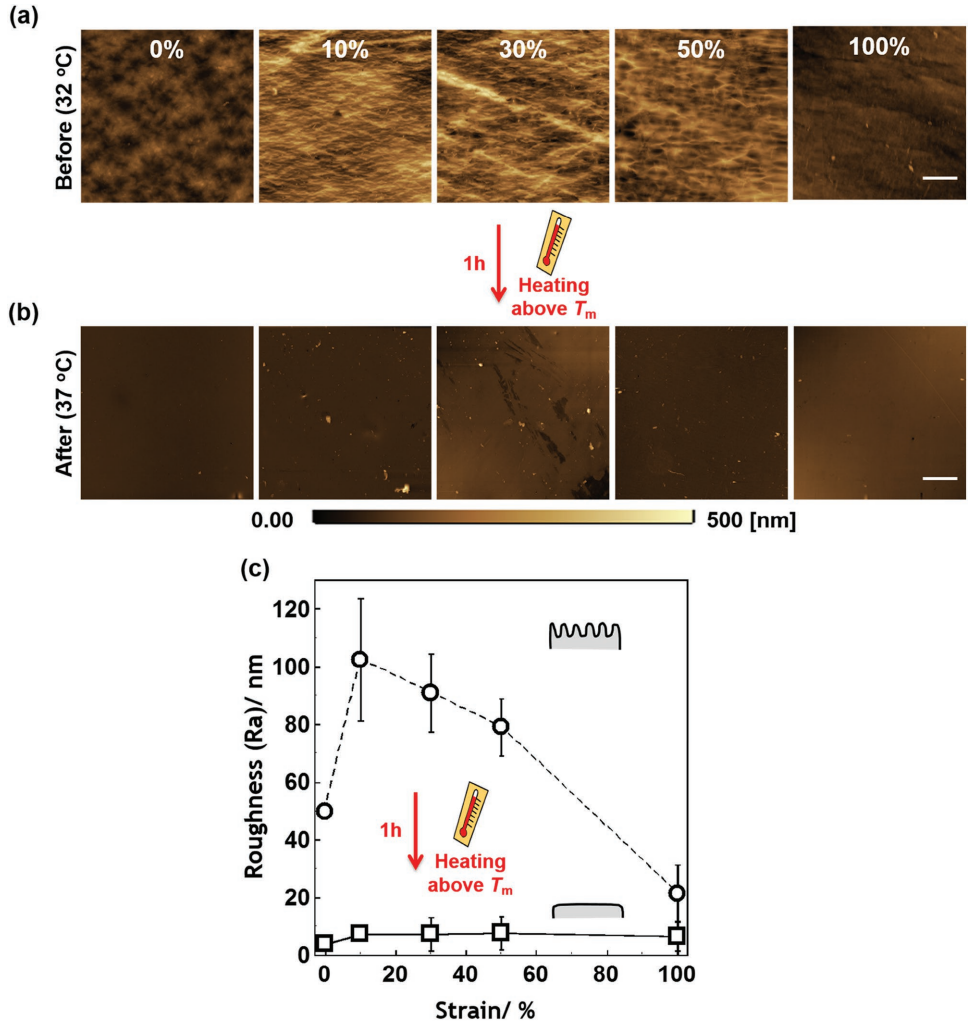

Figure 3. Effect of shape-memory activation on surface morphology of strain fixed films. 2D surface images (50 µm× 50 µm) of crosslinked PCL with various fixed strain were obtained by atomic force microscope (AFM) a) before and b) after shape-memory activation of 37 °C heating for 1 h (scale bars: 10 µm). c) Mean roughness (Ra) of crosslinked PCL with various fixed strains estimated from AFM images before (circular symbols) and after (square symbols) shape-memory activation of 37 °C heating for 1 h.

viable (Live/Dead assay) and cell numbers remained relatively constant even after shape-memory activation of crosslinked PCL with 100% fixed strain, samples that should induce the largest deformation to adhered cells (Figure S5 in the Supporting Information). Interestingly, increased cell alignment was observed on higher strain-fixed films, while little change in cell alignment was observed on lower strain-fixed films following shape-memory activation (Figure S6 in the Supporting Information). **Figure 6**a compares the average orientation angles of cells versus initial fixed strains before and after shape-memory activation. Before shape-memory activation, cells on the film with 10% and 30% fixed strain showed a clear indication of alignment around 11° ± 3° and 11° ± 2°, respectively. Cell orientation angles increased with increase of initial fixed strain became random for 100% strain (42° ± 3°). After shape-memory activation, on the other hand, cells on the film with 50% and 100% of fixed strain became highly oriented with angles of 10° ± 2° and 12° ± 3°, respectively. These results are consistent with the observed trends in dimensional change versus strain fixity in Figure 2b. Indeed, the dimensional changes for 100% strain-fixed film in elongation and perpendicular direction were almost 43% and 163% of their original sizes before shape-memory activation, respectively. We also evaluated the morphological changes of cells, which occur at an early stage of cytoskeletal arrangements. Figure 6b compares the normalized cell length of the long axis before and after shape-memory activation. For the film with 50% and 100% of fixed strain, the cell length increased after shape-memory activation due to the dimensional change of the film (Figure S7 in the Supporting Information). For the film with 10% and 30%, however, the cell length slightly decreased after shape-memory activation, suggesting that cells lost contact guidance when surface wrinkles disappeared.

2.4. Role of Shape-Memory Activation on Cell Morphology

To elucidate the differences of "surface" and "bulk" shape-memory effect on cell alignment, cells were continuously

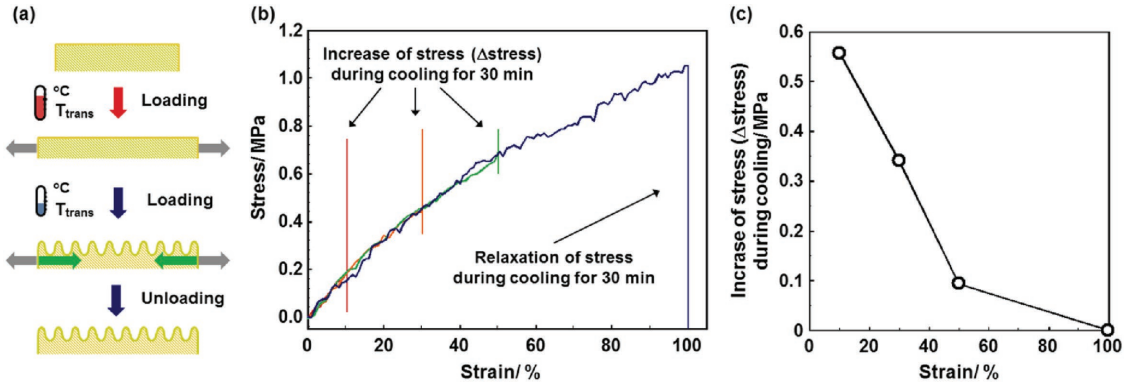

Figure 4. a) Schematic illustration of strain fixing process using tensile tester. Predetermined strain (0%–100%) was applied to the samples at 40 °C (above T_m). The applied strain was then fixed at 4 °C (below T_c) for 30 min of cooling. b) Sequential monitoring of stress–strain curves from elongation to fixing of applied strains. The additional stress increasing (Δstress) was observed during the fixing process of 10%, 30%, and 50% strain by cooling at 4 °C, although the stress was monotonically decreased during that of 100% strain. c) Stress increasing (Δstress) during the strain fixing process ploted against the applied strain. In applied strain of 100%, the Δstress was zero because the slight increase of stress during strain fixing process could not be detected.

cultured at 32 °C for 24 h following shape-memory activation. As seen in **Figure 7**a, the cell alignment dispersed again after 24 h. This result indicates that cells were first amenable to align by the dimensional change of the substrate, but spontaneously change their morphology with time. Figure 7b shows the morphological changes of the paraformaldehyde (PFA)-fixed cells on the substrate with 100% fixed strain, suggesting that the orientation and morphological transition were observed even in dead cells. However, no further changes were observed with time. Although the shape-memory transition of these samples was also associated with an elastic and compression modulus decrease from 26.4 ± 2.7 to 0.9 ± 0.1 MPa and 11.7 ± 0.1 to 5.8 ± 0.1 MPa (Table S1 and Figure S3 in the Supporting Information), respectively, they did not affect cell alignment in this study, as seen from cell morphology on the nonelongated (0% fixed strain) films in Figures 5 and 6.

3. Discussion

PCL-based SMPs remain one of the main classes of shape-memory materials for biological applications due to their biodegradability and biocompatibility characteristics. In this study, we comprehensively discussed a synergistic role of surface and bulk shape-memory effects on adhered fibroblasts using PCL-based SMP film with the shape-switching temperature near body temperature. In general, temporary surface nanopatterns are memorized by embossing the substrate surface with a lithographically patterned mold above the T_m. The memorized nanopatterns were fixed by releasing the compressive stress below the T_c. Alternatively, we employed a simple and versatile technique for generating temporary features on the PCL surfaces without the use of lithography. It is well known that surface wrinkle structures can be generated on elastomeric

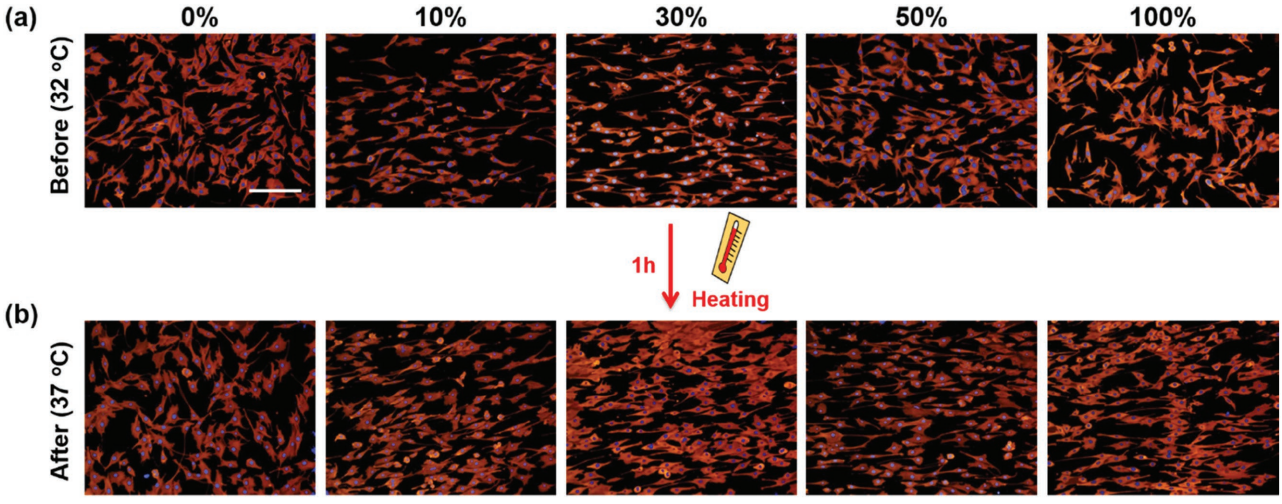

Figure 5. Effect of shape-memory activation on morphology and alignment of adhered cells on the strain fixed films. a) Fluorescent microscope images of NIH 3T3 fibroblasts seeded and cultured on the fibronectin-coated films with various fixed strain at 32 °C for 24 h. Cells were stained with F-actin (red) and nucleus (blue). b) The cells were then subjected to 37 °C heating for 1 h (scale bar: 200 μm).

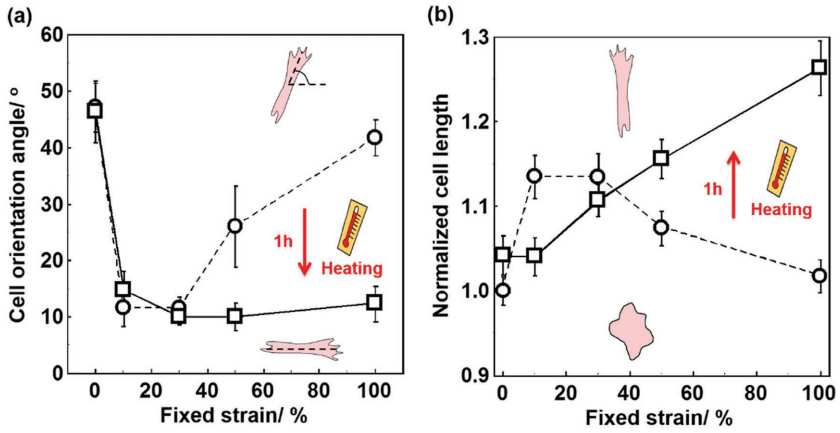

Figure 6. a) Orientation angles of cells cultured on the fibronectin-coated films with various fixed strain at 32 °C for 24 h (circular symbols). The cells were then subjected to 37 °C heating for 1 h (square symbols). Cell orientation angles were quantified by the analysis of immunostained images, and defined vertical direction to elongation as a 0°. b) Effect of shape-memory activation on morphological length of NIH3T3 fibroblasts. Cell lengths of long axis were quantified by the analysis of immunostained images before (circular symbols) and after (square symbols) shape-memory activation. All data were normalized by the length of cells on the original (fixed strain of 0%) film before shape-memory activation.

polymer substrates covered with a thin layer of metals.[40–42] The formation mechanism of this type of surface structure is due to the mismatch of the volumetric contractions between the metal layer and the polymer substrate. In this study, we succeeded in spontaneous formation of aligned nanowrinkle structures on the PCL films without the use of any coating or deposition with a rigid thin layer (Figure 1b; Figure S4, Supporting Information). In our system, this rigid layer should be formed by crystallization of PCL chains. In the cold crystallization process, crystallization rate at the surface of films is faster than in the bulk;[43] the differences between surface and bulk crystallization kinetics drives nanowrinkle formation. In addition, we believe that the contraction stress during the cooling process induced a drag on the PCL film depending on the applied strain that influences the expansion coefficient of the stretched sample at temperature above T_m and below T_c and volume changes in crystallization during the cooling process (Figure 4b,c).[27] This generated the compressive stress that triggered the generation of aligned surface nanowrinkle structures because the anisotropic volume changes from amorphous to crystal phase during the cooling process under applied stress. The film might form nanowrinkles perpendicular to the elongation direction to relax and reduce the increased stress during the cooling process. The nanowrinkle formation in this system is a novel phenomenon, different from other systems offering controlled shape-memory effects.[42,44] Thus, this method for generating surface nanowrinkle structures offers many advantages due to the simple, versatile, and experimentally straightforward technique that does not require chemical deposition with metals or photolithographic fabrication processes.

We investigated how surface morphology, dimensional change, as well as alterations in mechanics of substrates underneath adhered cells dynamically influence their orientation and adhesion morphology using the PCL films with nanowrinkles. Recent evidence suggests that mechanostructural properties of the extracellular matrix, particularly rigidity, topography,

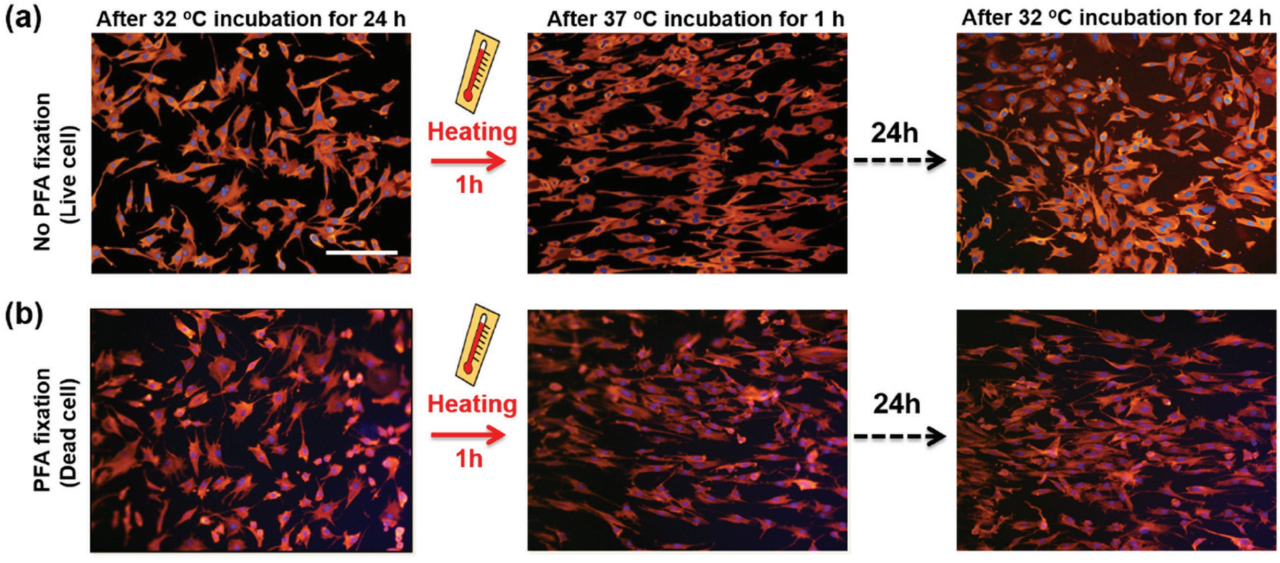

Figure 7. Effect of cell viability on the morphological changes in response to shape-memory activation. a) NIH 3T3 fibroblasts were cultured on the fibronectin-coated films with 100% strain at 32 °C for 24 h. Then the cultured cells were subjected to a 37 °C heat treatment for 1 h and cultured at 32 °C for 24 h. The cells were fixed by paraformaldehyde (PFA) and stained individually after each process. b) The prefixed (dead) cells after 24 h of incubation at 32 °C were continuously subjected to a 37 °C heat treatment for 1 h and cultured at 32 °C for 24 h (scale bar: 200 μm).

and dimension can mediate cell signaling, proliferation, differentiation, and migration. Actually, cells have adapted fully to topographical features of substrates and display corresponding morphology before shape-memory activation (Figure 5a). On the other hand, changes of cellular alignment and morphology responded to dynamic changes of substrates induced by shape-memory activation; these changes were strongly dependent on the fixed strain for temporally elongated substrates (Figure 5b). As for the orienting response of cells on the lower fixed strain films, little change was observed in their alignments after shape-memory activation. Although the dimensional change for the lower strain-fixed films was small, the surface wrinkle structures that completely transform from nanowrinkle to a flat should have significant effects on cell behavior. One of the plausible reasons is that the time required for cells to respond to topological features is relatively long as cytoskelatal rearrangements may involve several coupled intracellular signaling pathways. In our previous report, it took 24 h for aligned cells to disperse randomly when surface features transformed from grooves to flat.[32] Other studies have also showed that cells adapted to the surface features and displayed corresponding alignment for a period of 12–24 h regardless of cell types.[23,30,31] In fact, aligned cells on films with lower fixed strain dispersed again after 24 h of shape-memory activation as surface wrinkles disappeared.

On the other hand, in the "bulk" shape-memory activation, mechanical strain involved in large macroscopic deformation, rather than surface topography, induced the change of cell morphology and alignment. The transition kinetics for both "surface" and "bulk" shape-memory activation of substrate itself should be similar since both are based on the crystal-amorphous transition. Nevertheless, we clearly observed the kinetic difference of cellular (re)alignment behavior between "bulk" and "surface" shape-memory activation. Cellular response against bulk shape-memory activation, which can induce the dimensional change, was much faster (<1 h, Figures 5 and 6) than surface topographic effect (≈24 h). Therefore, "bulk" and "surface" shape-memory activation illicit cellular effect via different mechanisms. Several studies have shown that cells alter their shape dramatically in response to physical forces. Cyclic stretch, for example, increased tyrosine phosphorylation of cellular proteins followed by cell orienting along the perpendicular direction of the stretch axis.[45–47] These works highlight that shape deformation and realignment of cell, which are often involved in active remodeling of cytoskeleton and focal adhesion, can require several hours to respond to cyclic mechanical deformation. Under cyclic stretch, application frequency strongly influences cellular alignment as well;[47] therefore, it would be different with our monotonic mechanically deformed system based on bulk shape memory. In an approach that shares some similarity with our system, dynamic cell stretching device based on temperature-responsive hydrogels has been developed.[48] This device was modulated to stretch adhered cells by utilizing the swelling of hydrogels. The tensile strains applicable to cell were tunable by swelling time and covered over physiological range (≈0.2). Interestingly, cells gradually changed their shape in response to hydrogel deformation over relatively short response times (≈30 min). Although they did not focus on the cellular alignment, the kinetics of cell deformation are consistent with our results. Our approach can also apply to broad range of strain (>100%) in a more programmable manner. This feature might allow us to explore an interesting cellular behavior against more large deformation such as mimicking muscle stretching in vivo. In fact, the large dimensional change (≈100%) induced not only morphological change but also guiding cellular alignment, and bulk shape-memory approach is quite different from those previously reported.

Of special interest is that cell alignment was also observed for dead cells after dimensional change although the cell angles never disperse again. Thus, the rapid change of cellular alignment and morphology during the shape-memory activation can be attributed to the dynamic and asymmetric dimensional change of the substrate. In other words, cells were passively deformed and realigned as the substrate undergoes the large dimensional change, where it should not be involved in active remodeling of cytoskeleton and focal adhesion. Here, the conformation changes of polymer chains composed of crosslinked network from stretched lower entropy state to random coiled higher entropy state at molecular level caused by crystal-amorphous phase transition in response to temperature change were translated into dimensional change at macroscopic scale. Therefore, we could successfully manipulate the adhered cellular alignment and morphology by hierarchical regulation of molecular and macroscopic phenomenon, so-called "bulk" shape memory, regardless of cellular activity. Effects of "bulk" and "surface" shape-memory activations on cell alignment are summarized in **Figure 8**. For samples with lower fixed strain, a "surface" shape-memory activation (topographical change) plays a dominant role in cell alignment because their dimensional changes are small. In this study, we particularly focused on short-term responses of cells to shape-memory activation. Since surface topographical changes induce spontaneous cytoskeletal remodeling which requires longer time to propagate mechanical inputs from the topography, they have more significant effects on cell morphology at longer time periods. For samples with higher fixed strain, on the other hand, a "bulk" shape-memory activation (a dimensional change) plays a dominant role in cell alignment because their topographical changes are negligible. These results were significantly different from those previously reported.[36] We clearly observed the rapid cellular alignment and morphological transition in response to "bulk" shape-memory activation without observing significant cell detachment and inducing apoptosis. Our findings highlight the designed shape-memory system as a biocompatible dynamic cell culture platform that would potentially induce more biologically relevant mechanostructural changes.

4. Conclusion

This study elucidates the effects of dynamic changes in mechanostructural environments on fibroblasts adhesion, morphology, and alignment using shape-memory cell culture substrates that undergo programmed changes in both "surface" topography and "bulk" dimension as well as stiffness and compression modulus. We have developed biocompatible PCL films that have shape-memory transition temperature around

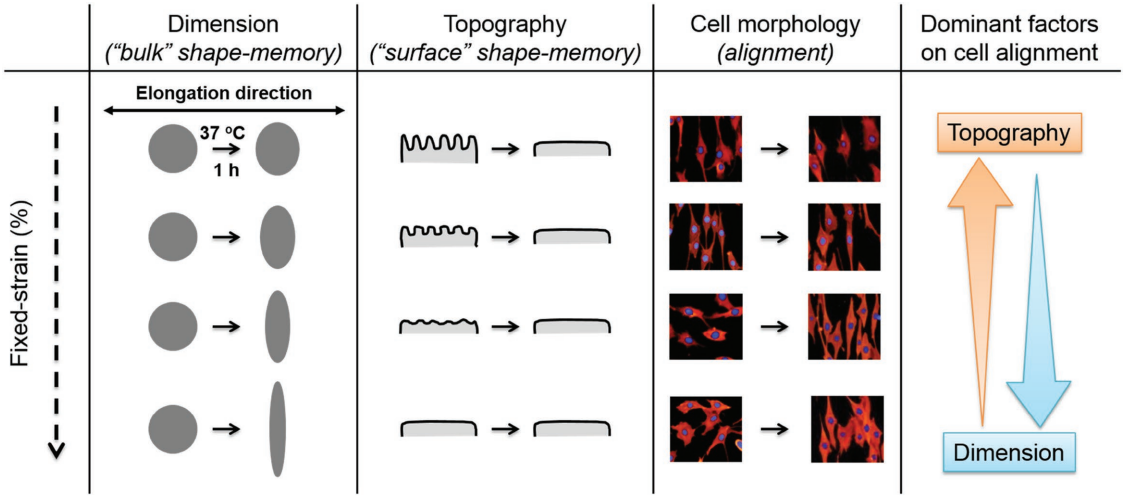

Figure 8. Summary of the role of "bulk" dimension change and "surface" topography change of crosslinked PCL by shape-memory activation. The cell alignment before and after shape-memory activation was determined by two dominant factors derived from surface (topography) and bulk (dimension) properties depended on the fixed strain of substrate in shape-memory culture platforms using crosslinked PCL.

a biologically relevant temperature and show a good surface wettability for cell culture. Surface topographic features and bulk dimensional changes were spontaneously programmed by simple stretching of the PCL films without the need of complicated deposition or fabrication processes. The surface features completely transformed from wrinkled to smooth surface by shape-memory activation. Shape-memory activation also triggered dimensional deformation in an initial fixed strain-dependent manner. A dynamic cell-orienting study demonstrated that topographical changes play a dominant role in cell alignment for samples with lower fixed strain, while dimensional changes play a dominant role in cell alignment for samples with higher fixed strain. As the proposed system is simple, versatile, and biocompatible, we forecast that these materials represent a milestone for the further study of spatiotemporal control of mechanostructural stimuli to direct cell fate and engineer the stem cell niche.

5. Experimental Section

Fabrication and Characterization of Shape-Memory PCL Films: The shape-memory PCL films were prepared by crosslinking tetrabranched PCL with acrylate end groups in the presence of linear PCL telechelic diacrylates according to a previously reported protocol.[32,37] Two-branched and four-branched PCL were synthesized by ε-caprolactone (CL) ring-opening polymerization that were initiated with tetramethylene glycol and pentaerythritol as initiators, respectively. Then, acryloyl chloride was reacted to the hydroxyl end group of the branched chains. The structures and the molecular weights were estimated by ^{1}H NMR spectroscopy (JEOL, Tokyo, Japan) (Figure S2, Supporting Information) and gel permeation chromatography (JASCO International, Tokyo, Japan), respectively. The average degrees of polymerization of each branch for two- and four-branch PCL were 18 and 10, respectively. The equimolar amounts of PCL macromonomers were then dissolved at 45 wt% in xylene containing twofold molar excess benzoyl peroxide to the end-group of macromonomers. The solution was injected between glass slides with a 0.2 mm thick Teflon spacer. Then thermal polymerization was carried out at 80 °C for 180 min to obtain the crosslinked PCL films. The thermal properties of the branched PCLs were measured by differential scanning calorimetry (6100, SEIKO Instruments, Chiba, Japan) at 5 °C min^{-1} of programming rate.

Shape Programming and Recovery of PCL Films: The fixing of applied strain was carried out by thermomechanical experiments.[27] A tensile tester (EZ-S 500N, Shimadzu, Kyoto, Japan) equipped with a thermo chamber (Chromato chamber M-600FN, TAITEC, Saitama, Japan) was used to allow simultaneous tensile test and thermal programs. The crosslinked PCL films were heated to 40 °C (above T_m) and elongated to the predetermined strain of 0%–100% (deforming process). The temperature was then cooled to 4 °C (below crystallization temperature T_c) for 30 min to fix applied strain while keeping the tensile strain (strain fixing process). This process also allowed the determination of the strain fixity rate R_f, as well as the strain recovery rate R_r. Dimensional changes of the PCL films before and after shape-memory activation were assessed by measuring their lateral and longitudinal lengths. The theoretical deformation was also modeled with an assumed Poisson's ratio of crosslinked PCL (≈0.46).[38,39]

Topographical Observation by AFM: The surfaces of strain-fixed PCL films were observed by AFM (SPM-9500J3, Shimadzu Co., Kyoto, Japan) with noncontact mode using Si_3N_4 cantilever (spring constant; 42 N m^{-1}), and the sample temperature was controlled using a thermo controller. The surface roughness (R_a) before and after shape-memory activation was estimated from AFM scans on 50 × 50 μm^2 area.

Cell Culture on PCL Films: Prior to cell cultivation, the strain-fixed PCL films were coated with 10 μg mL^{-1} fibronectin and equilibrated in a 32 °C incubator for 1 h. NIH 3T3 fibroblasts were then seeded at a density of 1.5 × 10^4 cells cm^{-2} on the strain-fixed PCL films and cultured in Dulbecco's modified Eagle's medium in the presence of 10% fetal bovine serum and 1% antibiotics at 32 °C. For shape-memory activation experiments, the cells were transferred to a 37 °C incubator after 24 h of incubation at 32 °C. The cells were subjected to a 37 °C heat treatment for 1 h. The cell morphology before and after shape-memory activation was monitored and imaged using a phase contrast microscope (Olympus IX71, Tokyo, Japan). Cell orientation angles were quantified by the analysis of immunostained images. Cells were fixed with 4% paraformaldehyde and treated with Rhodamine phalloidin for F-actin staining and DAPI for nucleus staining. The orientation angle of an individual cell was determined as the angle against the perpendicular direction to tensile direction. Elongation of cells was also assessed by measuring the length of the long axis.

Supporting Information

Supporting Information is available from the Wiley Online Library or from the author.

Acknowledgements

The authors would like to express their gratitude to the Grant-in-Aid for Challenging Exploratory Research (23651142) from the Ministry of Education, Culture, Sports, Science and Technology (MEXT) Japan, and to the MANA Foundry for the use of clean room facilities and equipment. This research was also partially granted by the Japan Society for the Promotion of Science (JSPS) through the "Funding Program for World-Leading Innovative R&D on Science and Technology (FIRST Program)," initiated by the Council for Science and Technology Policy (CSTP). K. Uto was partially supported by JSPS Postdoctoral Fellowship for Research Abroad for the present work at University of Washington, USA. The authors are grateful to Dr. John M. Hoffman (Stratos Genomics Inc. in USA) for continued and valuable discussion.

Received: December 19, 2016
Published online:

[1] D. E. Ingber, *Prog. Biophys. Mol. Bio.* **2008**, *97*, 163.
[2] D. E. Ingber, *Int. J. Dev. Biol.* **2006**, *50*, 255.
[3] A. J. Engler, *J. Cell Biology* **2004**, *166*, 877.
[4] A. J. Engler, S. Sen, H. L. Sweeney, D. E. Discher, *Cell* **2006**, *126*, 677.
[5] K. Y. Suh, D. H. Kim, E. A. Lipke, P. Kim, R. Cheong, S. Thompson, M. Delannoy, L. Tung, A. Levchenko, *Proc. Natl. Acad. Sci. USA* **2010**, *107*, 565.
[6] D. Y. Kim, M. H. You, M. K. Kwak, D. H. Kim, K. Kim, A. Levchenko, K. Y. Suh, *Biomacromolecules* **2010**, *11*, 1856.
[7] E. K. F. Yim, S. W. Pang, K. W. Leong, *Exp. Cell Res.* **2007**, *313*, 1820.
[8] H. L. Khor, Y. Kuan, H. Kukula, K. Tamada, W. Knoll, M. Moeller, D. W. Hutmacher, *Biomacromolecules* **2007**, *8*, 1530.
[9] C. Heinemann, S. Heinemann, A. Lode, A. Bernhardt, H. Worch, T. Hanke, *Biomacromolecules* **2009**, *10*, 1305.
[10] A. R. Costa-Pinto, V. M. Correlo, P. C. Sol, M. Bhattacharya, P. Charbord, B. Delorme, R. L. Reis, N. M. Neves, *Biomacromolecules* **2009**, *10*, 2067.
[11] C. A. DeForest, K. S. Anseth, *Annu. Rev. Chem. Biomol. Eng.* **2012**, *3*, 421.
[12] J. A. Burdick, W. L. Murphy, *Nat. Commun.* **2012**, *3*, 1269.
[13] M. W. Tibbitt, K. S. Anseth, *Sci. Transl. Med.* **2012**, *4*, 160ps24.
[14] C. A. DeForest, D. A. Tirrell, *Nat. Mater.* **2015**, *14*, 523.
[15] C. A. DeForest, K. S. Anseth, *Angew. Chem., Int. Ed.* **2012**, *51*, 1816.
[16] G. M. Hoben, E. J. Koay, K. A. Athanasiou, *Stem Cells* **2008**, *26*, 422.
[17] P. Nardo, M. Minieri, A. Ahluwalia, *Stem Cell Engineering. vol 41. Differentiative micro- and macroenvironmen*, **2011**, Springer, Berlin, 41e59.
[18] M. Yamato, Y. Akiyama, J. Kobayashi, J. Yang, A. Kikuchi, T. Okano, *Prog. Polym. Sci.* **2007**, *32*, 1123.
[19] N. Matsuda, T. Shimizu, M. Yamato, T. Okano, *Adv. Mater.* **2007**, *19*, 3089.
[20] M. Ebara, M. Yamato, T. Aoyagi, A. Kikuchi, K. Sakai, T. Okano, *Adv. Mater.* **2008**, *20*, 3034.
[21] M. Ebara, M. Yamato, M. Hirose, T. Aoyagi, A. Kikuchi, K. Sakai, T. Okano, *Biomacromolecules* **2003**, *4*, 344.
[22] M. Ebara, M. Yamato, T. Aoyagi, A. Kikuchi, K. Sakai, T. Okano, *Biomacromolecules* **2004**, *5*, 505.
[23] M. T. Lam, W. C. Clem, S. Takayama, *Biomaterials* **2008**, *29*, 1705.
[24] H. Y. Yoshikawa, F. F. Rossetti, S. Kaufmann, T. Kaindl, J. Madsen, U. Engel, A. L. Lewis, S. P. Armes, M. Tanaka, *J. Am. Chem. Soc.* **2011**, *133*, 1367.
[25] M. Guvendiren, J. A. Burdick, *Nat. Commun.* **2012**, *3*, 792.
[26] C. Yang, M. W. Tibbitt, L. Basta, K. S. Anseth, *Nat. Mater.* **2014**, *13*, 645.
[27] A. Lendlein, S. Kelch, *Angew. Chem., Int. Ed.* **2002**, *41*, 2035.
[28] M. Behl, M. Y. Razzaq, A. Lendlein, *Adv. Mater.* **2010**, *22*, 3388.
[29] T. Xie, *Nature* **2010**, *464*, 267.
[30] J. H. Henderson, K. A. Davis, K. A. Burke, P. T. Mather, *Biomaterials* **2011**, *32*, 2285.
[31] D. M. Le, K. Kulangara, A. F. Adler, K. W. Leong, V. S. Ashby, *Adv. Mater.* **2011**, *23*, 3278.
[32] M. Ebara, K. Uto, N. Idota, J. M. Hoffman, T. Aoyagi, *Adv. Mater.* **2012**, *24*, 273.
[33] Q. Shou, K. Uto, W.-C. Lin, T. Aoyagi, M. Ebara, *Macromol. Chem. Phys.* **2014**, *215*, 2473.
[34] M. Ebara, K. Uto, N. Idota, J. M. Hoffman, T. Aoyagi, *Int. J. Nanomed.* **2014**, *9*, 117.
[35] M. Ebara, M. Akimoto, K. Uto, K. Shiba, G. Yoshikawa, T. Aoyagi, *Polymer* **2014**, *55*, 5961.
[36] S. Neuss, I. Blomenkamp, R. Stainforth, D. Boltersdorf, M. Jansen, N. Butz, A. Perez-Bouza, R. Knüchel, *Biomaterials* **2009**, *30*, 1697.
[37] K. Uto, K. Yamamoto, S. Hirase, T. Aoyagi, *J. Control. Release* **2006**, *110*, 408.
[38] S. Iannace, N. De Luca, L. Nicolais, C. Carfagna, S. J. Huang, *J. Appl. Polym. Sci.* **1990**, *41*, 2691.
[39] C. Y. Wan, B. Q. Chen, *J. Mater. Chem.* **2012**, *22*, 3637.
[40] C. M. Stafford, C. Harrison, K. L. Beers, A. Karim, E. J. Amis, M. R. VanLandingham, H.-C. Kim, W. Volksen, R. D. Miller, E. E. Simonyi, *Nat. Mater.* **2004**, *3*, 545.
[41] N. Bowden, S. Brittain, A. G. Evans, J. W. Hutchinson, G. M. Whitesides, *Nature* **1998**, *393*, 146.
[42] J. Li, Y. An, R. Huang, H. Jiang, T. Xie, *ACS Appl. Mater. Interfaces* **2012**, *4*, 598.
[43] Q. Zia, E. Ingolič, R. Androsch, *Colloid. Polym. Sci.* **2010**, *288*, 819.
[44] P. Yang, R. M. Baker, J. H. Henderson, P. T. Mather, *Soft Matter* **2013**, *9*, 4705.
[45] X. R. Sai, K. Naruse, M. Sokabe, *J. Cell Sci.* **1999**, *112*, 1365.
[46] K. Furuya, M. Sokabe, S. Furuya, *J. Cell Sci.* **2005**, *118*, 3289.
[47] Y. Kamotani, T. Bersano-Begey, N. Kato, Y.-C. Tung, D. Huh, J. W. Song, S. Takayama, *Biomaterials* **2008**, *29*, 2646.
[48] D. Chen, R. D. Hyldahl, R. C. Hayward, *Lab Chip* **2015**, *15*, 1160.